Semi-Lagrangian Transport Algorithms for the Shallow Water Equations in Spherical Geometry

J.B. Drake and P.H. Worley
N. M. Nachtigal
*Oak Ridge National Laboratory**

D.L. Williamson
National Center for Atmospheric Research†

Abstract

Global atmospheric circulation models (GCM) typically have three primary algorithmic components: columnar physics, spectral tranform, and semi-Lagrangian transport. In this study, several varients of a SLT method are studied in the context of test cases for the shallow water equations in spherical geometry. A grid point formulation is used with implicit, semi-implicit or explicit time integration techniques based three time level differencing. The spatial error is minimized by using a spectral approximation of derivatives.

1 Introduction

The semi-Lagrangian transport (SLT) method is used in GCMs, for example, to advect moisture. The method updates the value of the moisture field at

*This research was supported by the Atmospheric and Climate Research Division, Office of Energy Research, U.S. Department of Energy under contract DE-AC05-84OR21400 with Lockheed Marietta Energy Research Inc.

†Sponsored by the National Science Foundation.

a grid point (the arrival point, A) by first establishing a trajectory through which the particle arriving at A has moved during the current timestep ($2\Delta t$). This trajectory is found iteratively using the interpolated velocity field at the midpoint, M, of the trajectory. From this midpoint the departure point, D, is calculated and the moisture field is interpolated at D using shape preserving interpolation.

Numerically integrating the differential equation along the particle path involves several approximations in addition to the interpolations which are used in a SLT method. Some terms may be evaluated at the midpoint of the trajectory while others are averaged in space or time from values at the arrival and departure points. In this study we examine the approximations in the context of test cases for the shallow water equations on a sphere.

Three time integration algorithms are studied resulting from the evaluation of terms at different time levels, explicit (EX), semi-implicit(SI) and implicit(IM). Further approximations result from spatial evaluation of terms at the midpoint (MID) of the trajectory or by spatial averages (SA). This gives a total of six distinct algorithms, EX-SA, EX-MID, SI-SA, SI-MID, IM-SA and IM-MID.

Of particular concern is the truncation error of the SA-approximation. Since it depends on the length of the trajectory we are interested in how it interacts with the horizontal resolution used for the interpolation of fields and for the evaluation of derivatives. To minimize the approximation error in the evaluation of gradient and divergence terms, a spectral approximation has been used. This allows us to observe the time truncation errors.

The choice of algorithm also implies a particular splitting of the geostrophic balance equation. For shallow water models and climate models or weather models, the geostrophic terms of the momentum equation are most significant. If the numerical approximation is unable to represent a geostrophic balance accurately, then there seems little reason use it. So attention will be paid to the accuracy of the methods when the analytic solution of the equations is a geostrophic balance.

In order to carry out this study, we departed from the conventional computationally efficient algorithm which uses the spectral method for evaluation of terms of the equations and for fast solution of the Helmholtz equation arising in the semi-implicit approximation. The implicit algorithm does not result in a simple Helmholtz problem and a more general solver strategy is needed. In this regard we introduce the Quasi-Mimimial Residual interative solver for the linear algebraic systems that are encountered. This solver turns out to be surprisingly efficient, but the point of our study is not computational efficiency but rather accuracy and the understanding of the implications of different approximations.

2 Shallow Water Equations on the Sphere

The shallow water equations in advective form are

$$\frac{d\mathbf{v}}{dt} = -f\vec{k} \times \mathbf{v} - \nabla\phi + \mathbf{S}_{\mathbf{v}} \tag{1}$$

$$\frac{d\phi^*}{dt} = -\phi^*\nabla\cdot\mathbf{v} + S_\phi \tag{2}$$

The vector $\mathbf{v} = u\vec{i} + v\vec{j}$ is the horizontal vector velocity and is always orthogonal to the unit vector $\vec{k}$ in the radial direction. The free surface geopotential is denoted by $\phi = \phi^* + \phi_s = g(h^* + h_s)$, where g is the gravitational acceleration and h^* is the height of the free surface above the bottom height, h_s. The bottom surface height can be used to specify orography as a time invariant function. The Coriolis parameter $f = 2\Omega \sin\theta$ incorporates the effect of rotatation of the sphere with angular velocity Ω at latitude θ. In the shallow water equations a source term $\mathbf{S}_{\mathbf{v}}$ and S_h are included as a formality. The equations require no boundary conditions but are posed with initial conditions on $\mathbf{v}$ and ϕ.

The substantial derivative is given by

$$\frac{d}{dt} = \frac{\partial}{\partial t} + \mathbf{v} \cdot \nabla. \tag{3}$$

The gradient operator in spherical coordinates is given by

$$\nabla = \frac{\vec{i}}{a\cos\theta}\frac{\partial}{\partial\lambda} + \frac{\vec{j}}{a}\frac{\partial}{\partial\theta}. \tag{4}$$

The divergence operator on the sphere in the lon-lat coordinate system is defined by

$$\nabla \cdot \mathbf{v} = \frac{1}{a\cos\theta}\left(\frac{\partial u}{\partial\lambda} + \frac{\partial v\cos\theta}{\partial\theta}\right). \tag{5}$$

3 Semi-Implicit, Semi-Lagrangian Formulation

A three time level semi-Lagrangian method for the shallow water equations has been described in Ritchie [8]. An extension of this using spatial averages in semi-implicit, semi-Lagrangian schemes is discussed in [10]. For meterological models the form of their method is based on a division of terms in the equations between those involved in the fast moving waves, e.g. gravity waves, and the slower moving Rossby waves. Let G denote the fast moving wave terms and R the slower wave terms. Then an advected scalar field F is represented by the equation

$$\frac{dF}{dt} + G = R. \tag{6}$$

Let subscripts $()_A$, $()_M$ and $()_D$ represent quantities evaluated at the arrival point, midpoint and departure point, respectively. Let superscripts $\tau - 1$, τ and $\tau + 1$ represent the three time levels at which quantites are evaluated.

Integrating the equation (6) along the trajectory between the departure point and the arrival point

$$\int_{t^{\tau-1}}^{t^{\tau+1}} \frac{dF}{dt} + \int_{t^{\tau-1}}^{t^{\tau+1}} G = \int_{t^{\tau-1}}^{t^{\tau+1}} R. \tag{7}$$

The first term reduces exactly by the fundamental theorem of calculus,

$$\int_{t^{\tau-1}}^{t^{\tau+1}} \frac{dF}{dt} = F_A^{\tau+1} - F_D^{\tau-1}, \tag{8}$$

while the G and R terms must be approximated using some quadrature rule. Interesting quadrature rules are

$$\begin{aligned} \int_{t^{\tau-1}}^{t^{\tau+1}} G &= 2\Delta t G_M^{\tau} + O(\Delta t^2) \quad \text{midpoint} \\ & \quad \Delta t(G_A^{\tau+1} + G_D^{\tau-1}) + O(\Delta t^3) \quad \text{trapezoidal} \\ & \quad \frac{\Delta t}{3}(G_A^{\tau+1} + 4G_M^{\tau} + G_D^{\tau-1}) + O(\Delta t^5) \quad \text{Simpson} \end{aligned}$$

The trapeziodal rule for G and a midpoint rule for R gives the following semi-implicit formulation.

$$\frac{F_A^{\tau+1} - F_D^{\tau-1}}{2\Delta t} + \frac{G_A^{\tau+1} + G_D^{\tau-1}}{2} = R_M^{\tau}. \tag{9}$$

These three time level "centered" approximations result in an $O(\Delta t)$ approximation to (6); the approximation to F is $O(\Delta t^2)$. This approximation is the basis for most three level semi-implicit SLT methods. The review article by Staniforth and Côté [9] discusses the development of the SLT method and some of its applications. We note in particular that Ritchie's [8] three level spectral shallow water model was based on this approximation.

Another approximation can be obtained by replacing the R_M^τ term with a spatial average at time level τ. Then the spatially averaged, semi-implicit, semi-Lagrangian scheme for equation (6) is,

$$\frac{F_A^{\tau+1} - F_D^{\tau-1}}{2\Delta t} + \frac{G_A^{\tau+1} + G_D^{\tau-1}}{2} = \frac{R_A^\tau + R_D^\tau}{2}, \tag{10}$$

or

$$F_A^{\tau+1} + \Delta t G_A^{\tau+1} = F_D^{\tau-1} + \Delta t[R_A^\tau + R_D^\tau - G_D^{\tau-1}] \equiv N. \tag{11}$$

The arrival and departure components of N can be defined in terms of the R's and G's as

$$N_A \equiv \Delta t R_A^\tau \tag{12}$$

and

$$N_D \equiv F_D^{\tau-1} + \Delta t[R_D^\tau - G_D^{\tau-1}]. \tag{13}$$

This approximation has been shown to be advantagous in numerical weather prediction models [10] because it reduces distortion produced by topographically forced waves. The spatial average introduces a further approximation error $O(\Delta x^2)$ where Δx is the length of the trajectory and not the spatial resolution. But since the trajectory length is proportional to the time step Δt this is thought to be an acceptable error. In this paper we study this approximation and the various assignments of terms in the simple context of the shallow water equations. A set of test cases, some with analytic solutions, can then be used to understand the properties of the approximation.

The assignment of terms of the shallow water equations to G and R results in different numerical algorithms. If we take $G \equiv 0$, then the algorithm is *explicit* in time. The explicit method requires small timesteps to stabilize the gravity wave components of the solution. A *semi-implicit* method results by assigning selected terms to G, terms that give rise to the gravity waves. In the momentum equation (1) the gravity wave component is identified with the $\nabla\phi$ term and the Coriolis term is identified with the R. We take

$$R = \begin{pmatrix} fv - \frac{1}{a\cos\theta}\frac{\partial\phi_s}{\partial\lambda} + S_u \\ -fu - \frac{1}{a}\frac{\partial\phi_s}{\partial\theta} + S_v \\ -(\phi' + \phi_s)\nabla\cdot\mathbf{v} + S_\phi \end{pmatrix}, \tag{14}$$

$$G = \begin{pmatrix} \frac{1}{a\cos\theta}\frac{\partial\phi'}{\partial\lambda} \\ \frac{1}{a}\frac{\partial\phi'}{\partial\theta} \\ \phi\nabla\cdot\mathbf{v} \end{pmatrix} \tag{15}$$

where $\phi = \bar{\phi} + \phi_s + \phi'$ and $\bar{\phi}$ is a constant reference value.

Another algorithm is obtained by moving the Coriolis term into the implicit G.

$$R = \begin{pmatrix} -\frac{1}{a\cos\theta}\frac{\partial\phi_s}{\partial\lambda} + S_u \\ -\frac{1}{a}\frac{\partial\phi_s}{\partial\theta} + S_v \\ -(\phi' + \phi_s)\nabla\cdot\mathbf{v} + S_\phi \end{pmatrix}, \tag{16}$$

$$G = \begin{pmatrix} \frac{1}{a\cos\theta}\frac{\partial\phi'}{\partial\lambda} - fv \\ \frac{1}{a}\frac{\partial\phi'}{\partial\theta} + fu \\ \phi\nabla\cdot\mathbf{v} \end{pmatrix}. \tag{17}$$

This will be called the *implicit* algorithm reserving the terminology *fully implicit* for the case of $R \equiv 0$.

In vector form, the semi-implicit shallow water formulation is,

$$\mathbf{v}_A^{\tau+1} + \Delta t\nabla\phi'^{\tau+1}_A = \mathbf{v}_D^{\tau-1} - \Delta t[(f\vec{k}\times\mathbf{v})^\tau_A + (f\vec{k}\times\mathbf{v})^\tau_D + \nabla\phi'^{\tau-1}_D] \equiv N_{\mathbf{v}}, \tag{18}$$

and

$$\phi'^{\tau+1}_A + \Delta t\bar{\phi}\nabla\cdot\mathbf{v}_A^{\tau+1} = \phi'^{\tau-1}_D - \Delta t[(\phi'\nabla\cdot\mathbf{v})^\tau_A + (\phi'\nabla\cdot\mathbf{v})^\tau_D + \bar{\phi}\nabla\cdot\mathbf{v}_D^{\tau-1}] \equiv N_\phi, \tag{19}$$

4 Grid Point Based Formulations

The solution of the semi-implicit, semi-Lagrangian equations (11) requires the solution of an elliptic equation. A Helmholtz equation can be derived from equations (18) and (19). By taking the divergence $\nabla \cdot ()$ of the momentum equation, and substituting into equation (19), an equation for ϕ' results:

$$\phi'^{\tau+1}_A - \Delta t^2 \bar{\phi} \nabla^2 \phi'^{\tau+1}_A = N_\phi - \Delta t \bar{\phi} \nabla \cdot N_{\mathbf{V}} \equiv H_\phi. \tag{20}$$

Once ϕ' is determined from this equation, the velocity can be found from equation (18).

The solution of the Helmholtz equation by the spectral transform method is one choice among many. If the spectral transform has not been used to evaluate the gradient and divergence operators, its use for the solution of the Helmholtz system is not computationally efficient. So for grid point based formulations, an iterative method for the solution of the elliptic system is prefered. The conjugate gradient algorithm [6], has been widely used for the solution of symmetric, positive definite linear systems. The appropriate use of preconditioners can greatly enhance the speed of convergence yielding a relatively fast method. Further, the semi-Lagrangian equations introduce an $O(\Delta t^2)$ error so it is not necessary to solve the Helmholtz problem exactly, i.e. to machine precision. An iterative method can be terminated when a desired accuracy has been reached. This also allows some computational efficiency.

For the implicit algorithm, the Coriolis term must be taken into account in the solution of the system of equations (11). If this term is carried through in deriving an elliptic equation for ϕ' there results

$$\phi'^{\tau+1}_A - \Delta t^2 \bar{\phi} \nabla \cdot (C(\theta) \nabla \phi'^{\tau+1}_A) = N_\phi - \Delta t \bar{\phi} \nabla \cdot (C(\theta) N_{\mathbf{V}}) \equiv H_\phi. \tag{21}$$

In this equation $C(\theta)$ is the inverse of the matrix

$$\begin{pmatrix} 1 & \Delta t f \\ -\Delta t f & 1 \end{pmatrix}. \tag{22}$$

More generally, the non-symmetric equations (11) can be solved in their original form using the Quasi-Minimal Residual (QMR) iteration. Since the QMR method is relatively new and its application to flow problems somewhat novel [**?**], a brief explanation is warranted.

4.1 Transpose Free, Quasi-Minimal Residual Method

The transpose-free quasi-minimal residual method (TFQMR) was proposed by Freund in [2], and the implementation used was taken from the package

QMRPACK, by Freund and Nachtigal [5]. TFQMR belongs to the class of so-called Krylov subspace methods, of which the best known method is the conjugate gradients method (CG) of Hestenes and Stiefel for Hermitian, positive-definite matrices.

Given a nonsingular $N \times N$ matrix A, real or complex, a right-hand side vector b, and a starting guess x_0, Krylov subspace methods generate successive approximations x_n to the solution x of the linear system

$$Ax = b$$

by building a basis for the Krylov space $K_n(r_0, A)$ and then selecting an iterate from the shifted Krylov space $x_0 + K_n(r_0, A)$. Here, $r_0 = b - Ax_0$ is the initial residual, and $K_n(v, A)$ denotes the nth Krylov subspace generated by a vector v and the matrix A,

$$K_n(v, A) = \mathrm{span}\{v, Av, \ldots, A^{n-1}v\}.$$

The basis for the Krylov space is typically built using either the Arnoldi process or the Lanczos process. The Arnoldi process is equivalent to applying Gram-Schmidt orthogonalization to the set of vectors

$$\{r_0, Ar_0, \ldots, A^{n-1}r_0\}$$

and thus results in an orthonormal basis set, This makes it possible to select the optimal iterate x_n that has minimum residual norm; the corresponding algorithm is generalized minimal residual (GMRES). The drawback of the Arnoldi process is that work and storage requirements increase with the iteration number, eventually forcing a restart of the procedure. The Lanczos process is equivalent to applying two-sided Gram-Schmidt biorthogonalization to the two sets of vectors

$$\{r_0, Ar_0, \ldots, A^{n-1}r_0\} \quad \text{and} \quad \{\tilde{r}, A^T\tilde{r}, \ldots, (A^T)^{n-1}\tilde{r}\}$$

and thus results in a biorthogonal basis set. The biorthogonalization can be carried out using three-term recurrences, thus avoiding the growth of work and storage requirements encountered with the Arnoldi process. However, it is no longer possible to cheaply select the optimal iterate x_n that has minimum residual norm; instead, the quasi-minimal residual algorithms [4, 2, 5] compute an iterate satisfying a relaxed optimality condition, as will be shown shortly. The drawback of the Lanczos process is that the procedure may encounter division by zero or by extremely small numbers; the remedy — look-ahead Lanczos algorithms [3] — is known, but is not simple. An additional drawback of the Lanczos process is that it requires multiplications with A^T, which may not be easily available, especially if matrix-free algorithms are used to carry out the multiplication with A — as is the case for our application. Hence, we were limited to using one of the transpose-free Lanczos-based algorithms, and we selected TFQMR. A complete presentation of TFQMR is given in [2]; here, we will present only a brief summary of the algorithm.

TFQMR implicitly uses the Lanczos process to generate basis vectors for the Krylov space $K_n(r_0, A)$. However, by taking advantage of the biorthogonality of the basis and by manipulating the polynomial inner products underlying the Lanczos process, TFQMR replaces the multiplication with A^T required at each step of the Lanczos algorithm by a second multiplication with A. It thus generates, after n steps, two sets of vectors Y_n and W_{n+1},

$$\begin{aligned} Y_n &= [y_1 \quad y_2 \quad \cdots \quad y_n], \\ W_{n+1} &= [w_1 \quad w_2 \quad \cdots \quad w_n \quad w_{n+1}], \end{aligned}$$

such that

$$AY_n = W_{n+1}B_n,$$

where B_n is a lower bidiagonal $(n+1)\times n$ matrix of full column rank, and $w_1 = r_0 = b - Ax_0$. The vectors Y_n form a basis for the Krylov space $K_n(r_0, A)$, and they are updated using a separate two-term recurrence formula that also requires a multiplication with A at each step, for a total of two matrix-vector products per step. Unlike the standard Lanczos process, the transpose-free variant does not have look-ahead, so it is possible that the procedure may encounter a breakdown in the form of division by zero. Once the basis vectors are generated, the algorithm constructs iterates x_n of the general form

$$x_n = x_0 + Y_n z_n,$$

where z_n is an n-vector of coefficients. The corresponding residuals r_n are

$$\begin{aligned} r_n &= b - Ax_n = r_0 - AY_n z_n \\ &= W_{n+1}\left(e_1^{(n+1)} - B_n z_n\right), \end{aligned} \tag{23}$$

where $e_1^{(n+1)} = [1 \quad 0 \quad \cdots \quad 0]^T$ is of length $n+1$. The basic TFQMR algorithm computes the iterates x_n whose coefficient vectors z_n minimize the norm

$$\left\| e_1^{(n+1)} - B_n z_n \right\|_2 ,$$

which is just the coefficients of the expansion (23); this is where the name *quasi-minimal residual* comes from. It is possible to update the iterates x_n using short recurrences, so that the resulting algorithm requires, at each step, two matrix-vector products, two vector dot products, two vector norms, and storage for nine vectors.

5 Semi-Lagrangian Interpolations

Following Williamson [12] the $N_{\mathbf{V}}$ can be written,

$$N_{\mathbf{V}} = N_A^1 \vec{i}_A + N_A^2 \vec{j}_A + N_D^1 \vec{i}_D + N_D^2 \vec{j}_D \tag{24}$$

In this expression $\vec{i}_A$ is the unit vector in the first component direction at the arrival point, and similaraly for the other directional unit vectors. Following Bates *et. al.* [1], a relation between the direction vectors at the arrival point and the departure point is given by

$$\begin{aligned} \vec{i}_D &= \alpha_1 \vec{i}_A + \beta_1 \vec{j}_A \\ \vec{j}_D &= \alpha_2 \vec{i}_A + \beta_2 \vec{j}_A . \end{aligned} \tag{25}$$

In these expressions

$$\begin{aligned} \alpha_1 &= \cos(\lambda_A - \lambda_D) \\ \alpha_2 &= \sin\theta_D \sin(\lambda_A - \lambda_D) \\ \beta_1 &= -\sin\theta_A \sin(\lambda_A - \lambda_D) \\ \beta_2 &= \cos\theta_A \cos\theta_D + \sin\theta_A \sin\theta_D \cos(\lambda_A - \lambda_D) \end{aligned} \tag{26}$$

Using these expressions we can express equation (24)

$$\begin{aligned} N_U &= N_A^1 + \alpha_1 N_D^1 + \alpha_2 N_D^2 \\ N_V &= N_A^2 + \beta_1 N_D^1 + \beta_2 N_D^2 \end{aligned} \tag{27}$$

To be explicit, the individual terms for the semi-implicit algorithm are

$$
\begin{aligned}
N_A^1 &= \Delta t (fv)_A^\tau \\
N_A^2 &= -\Delta t (fu)_A^\tau \\
N_D^1 &= \left[u^{\tau-1} - \Delta t(-(fv)^\tau + \frac{1}{a\cos\theta}\frac{\partial \phi^{\tau-1}}{\partial \lambda}) \right]_D \\
N_D^2 &= \left[v^{\tau-1} - \Delta t((fu)^\tau + \frac{1}{a}\frac{\partial \phi^{\tau-1}}{\partial \theta}) \right]_D
\end{aligned} \tag{28}
$$

The interpolation of the values at the departure points must now be addressed. The following quantities in physical space must be interpolated at the departure points, $\mathbf{v}^{\tau-1}$, $\mathbf{v}^\tau$, ϕ^τ, $\phi^{\tau-1}$, (δ^τ, $\delta^{\tau-1}$), and $\nabla\phi^{\tau-1}$. With these quantities we can form the $N_{\mathbf{V}}$ and N_ϕ. Alternatively, the sums of terms invloved in N_D^1 and N_D^2 can be formed at the grid points and then interpolated to the departure points. This is computationally less expensive and introduces an error only on the order of the interpolation error.

The interpolations are calculated using a shape preserving tensor product interpolation scheme developed by Williamson and Rasch [13]. A quasi-cubic interpolant is used for all fields involved in the calculation of the N's.

The departure point calculation integrates the equation backwards in time along the trajectory from the arrival point using

$$
\frac{d\mathbf{x}}{dt} = \mathbf{v} \tag{29}
$$

The midpoint of the trajectory is calculated using

$$
\begin{aligned}
\lambda_M &= \lambda_A - \Delta t u(\lambda_M, \theta_M) \\
\theta_M &= \theta_A - \Delta t v(\lambda_M, \theta_M).
\end{aligned} \tag{30}
$$

At each step of this iteration for the midpoint, the velocity field must be interpolated to the current estimate of the midpoint. Previous work [9] indictes that a linear interpolation of the velocities is adequate for accuracy in the solution of the shallow water equations. In a baroclinic model more accuracy may be needed. Lagrange cubic interpolation was used for velocities in this study.

Once the midpoint iteration has converged the departure point is calculated using,

$$\begin{aligned} \lambda_D &= \lambda_A - 2\Delta t u(\lambda_M, \theta_M) \\ \theta_D &= \theta_A - 2\Delta t v(\lambda_M, \theta_M). \end{aligned} \tag{31}$$

The explicit treatment of the vector sums on the sphere includes a treatment of the metric terms of the advection operator. If the u and v equations are treated simply as advection in spherical coordinates, then the u equation includes a term $uv \tan\theta/a$ and the v equation must include $u^2 \tan\theta/a$. The metric term also enters the geostrophic balance and so we note that the different splittings also split the treatment of the metric term.

5.1 Gridpoint SI and Implicit SLT

The grid point based algorithm would procede as follows: With values of $\mathbf{v}$, ϕ, $\nabla\phi'$, at time-levels τ and $\tau - 1$,

1. Calculate $N_{\mathbf{v}}$ and N_ϕ at the arrival points.
2. For each arrival point
   (a) Calculate the departure point (λ_D, θ_D), interpolating $\mathbf{v}_M$.
   (b) Interpolate N_D, evaluate the α's and β's used in equation (27), and calculate N's as the sum of arrival point and departure point values.
3. Evaluate H_ϕ in equation (20).
4. Solve the system (11) using the TFQMR iteration or use a fast Helmholtz solver with equation (20) for ${\phi'}_A^{\tau+1}$. If the elliptic equation for ${\phi'}_A^{\tau+1}$ alone has been solved, calculate $\mathbf{v}_A^{\tau+1}$ from $\nabla{\phi'}_A^{\tau+1}$ and equation (18).

6 Numerical Experiments and Results

The discussion will concentrate on the errors evident in the several schemes compared. We will concentrate on four sources of error: 1) the error associated with approximation of spatial derivatives, 2) the truncation error of the time stepping method, 3) the interpolation error of the semi-Lagrangian scheme, and 4) the error associated with computing trajectories in the semi-Lagrangian scheme. It will not always be possible to determine which is the dominant error.

For the numerical experiments reported here the gradient and the divergence operator were approximated using the spectral transform. Thus high accuracy of the spatial deriviatives is obtained uniformily through the experiments. This allows for the SLT approximations to be clearly seperated from the accuracy of the spatial derivative approximations.

The interpolation scheme is third order accurate in the spatial resolution but this error is componded if the departure points are computed inacurately. Of particular interest is the accuracy of the SLT approximations. Is there a problem with approximating the gradient terms in a different manner than the Coriolis terms as the semi-implicit algorithm does? What sort of accuracy degredation is expected with the increased timestep allowed by the implicit and semi-implicit SLT formulations?

A final complexity in the algorithms must also be introduced in comparision of numerical results. The schemes are not always stable. The explicit and semi-implicit methods are vulnerable to the leapfrog unstable mode in which the fields at even time levels become uncoupled from the fields at odd time levels. This mode can be suppressed by the application of the Asselin time filter. It will be noted where the use of the filter has been necessary to stabilize the computation.

Test cases are from the shallow water test suite of [11]. A non-SLT semi-implicit spectral shallow water code provides reference solutions for the test suite [7]. The cases can be used to characterize the numerical properties of a method and their appropriateness for numerical weather prediction and climate modeling. They provide a means of addressing accuracy as well as quality of solution in terms of conserved quantities.

6.1 Advection Test

Test case 1 is a pure advection problem in which a cosine bell is blown around the sphere under a constant velocity field. Since the velocity field is held constant throughout the simulation, only the explicit SLT algorithm (EX) is applicable. Figure 1 shows the simulated and exact profiles as the bell passes over the north pole. Figure 2 shows the simulated and exact

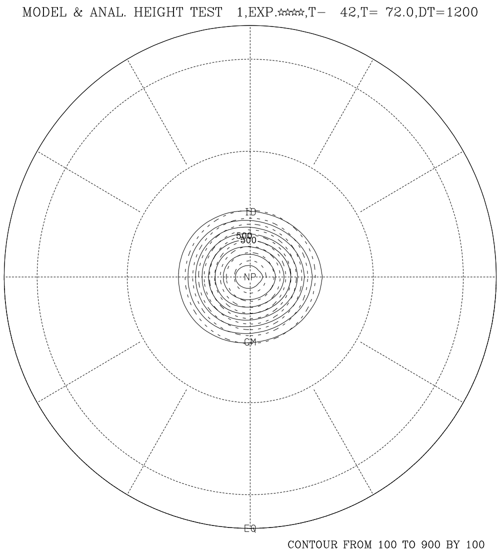

Figure 1: Cosine Bell ϕ, Test Case 1 at 3 Days, T42

profiles at the end of the 12 day simulation when the bell has returned to its starting position. The error at the end of the simulation is plotted in Figure 3.

The semi-Lagrangian method is relatively insensitive to the time step used. In Figure 4 we compare the accuracy of the explicit method with two different times steps and at different resolutions. The small timestep is not more accurate leading to the conclusion that the chief source of error is in the semi-Lagrangian interpolation.

6.2 Steady, Zonal Flow Test

Test case 2 is a steady, non-linear zonal flow rotated through an angle $\alpha = \frac{\pi}{4}$. It tests the ability of the code to maintain a steady state solution independent of the grid orientation and gives a good idea of the accuracy of the methods. The velocity and geopotential for this test case are exactly representable with the spherical harmonics of second order. So the local spherical harmonic approximations for the derivative operators are able to capture the steady

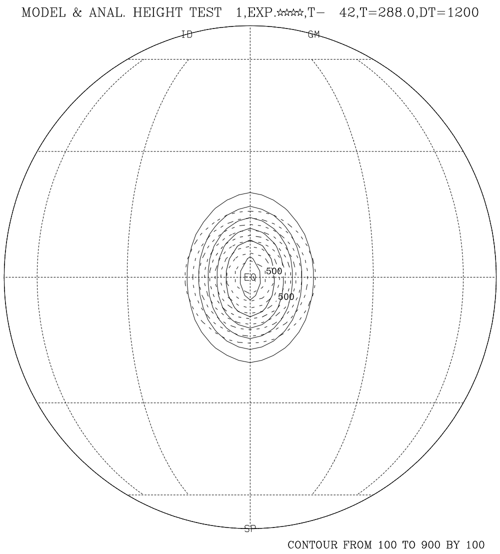

Figure 2: Cosine Bell ϕ, Test Case 1 at 12 Days, T42

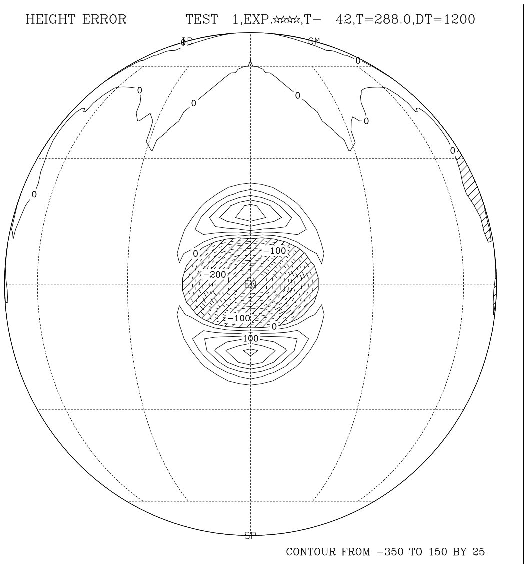

Figure 3: Error in ϕ, Test Case 1 at 12 Days, T42

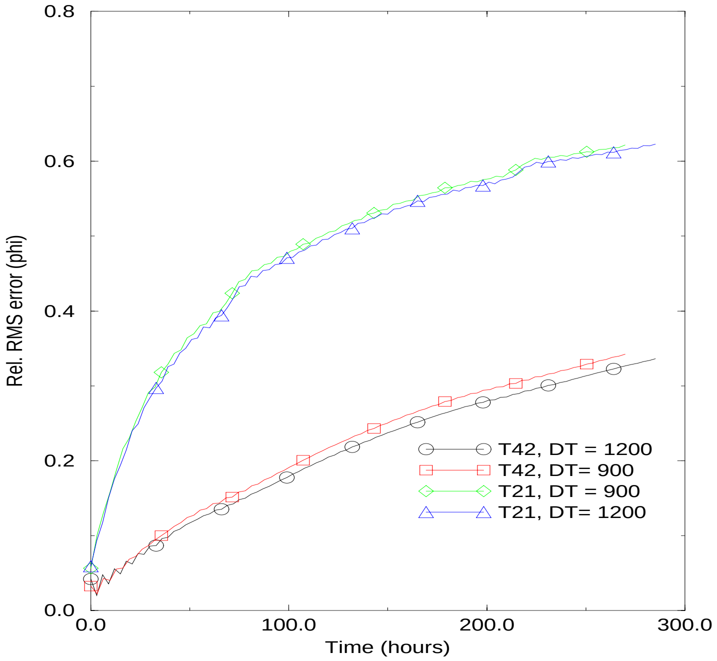

Figure 4: Relative RMS Error in ϕ, Test Case 1, T42 and T21

state solution extremely well.

The Asselin filter was used to stabilize the computation for several of the methods. Figure 5 shows the relative error in the geopotential as a function of time for all the schemes *without* the time filter. The explicit method and the implicit methods have better initial error than the semi-implicit method. Both these methods keep the geostrophic balance consistently at interpolation points while the semi-implicit method splits the balance term, approximates and then combines. The leap frog instability is evident in the explicit and semi-implicit methods point to the need for filtering.

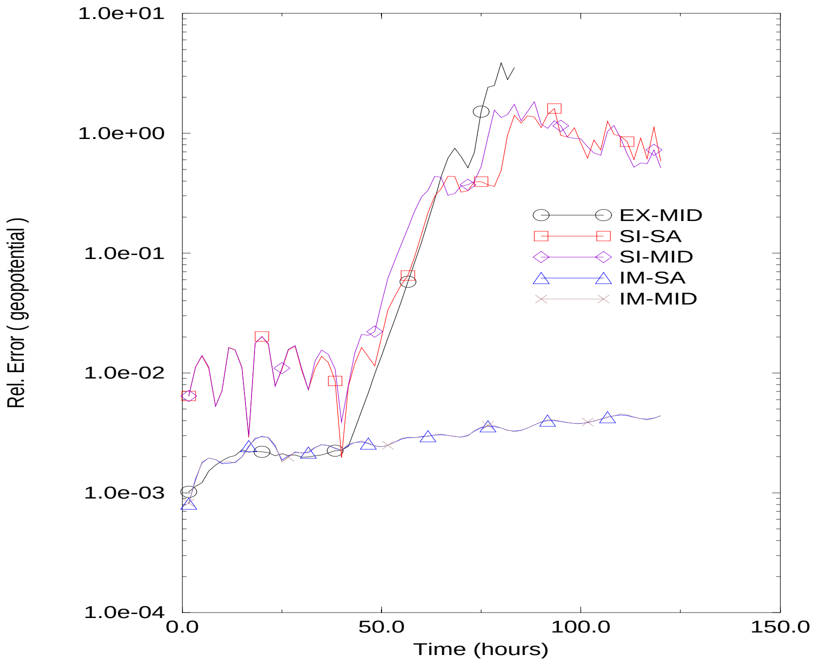

Figure 5: Non Filtered: Relative Max Error in ϕ, Test Case 2, T21

Figure **??** and **??** show the error, as a function of time, in the velocity (using the relative RMS error with the exact steady solution) and the RMS error in the height field, respectively.

The astrisk (*) on the method name in table 6 indicates that the Asselin time filter was used to stabilize the computation. Even with the filter, a time step of 900 seconds was required for stability indicating a CFL criteria limiting the timestep is in play. Error comparison between the explicit midpoint (EX-MID) and the explicit spatial average (EX-SA) indicate a smoothing

	$\Delta t = 1200$			$\Delta t = 1800$		
Method	$nI(\phi)$	$nI(\mathbf{v})$	Iterations	$nI(\phi)$	$nI(\mathbf{v})$	Iterations
EX-SA*	–	–	–	8.1e-2	2.7e-1	0
EX-MID*	–	–	–	1.7e-1	5.3e-1	0
SI-SA*	4.7e-3	7.6e-2	6	3.7e-3	6.0e-2	5
SI-MID*	4.6e-3	7.6e-2	6	4.5e-3	6.0e-2	5
IM-SA	4.4e-3	2.4e-2	7	4.1e-3	2.2e-2	5
IM-MID	3.3e-3	1.6e-2	7	4.1e-3	2.1e-2	5

Figure 6: Case 2: Error Summary at 5 days,$\Delta t = 1200$, T21

effect of the spatial average. The implicit method (IM) consistently yields higher accuracy than the semi-implicit for this case. The geopotential and velocity fields are exactly representable by the spherical harmonic basis for this case, and we expect little or no error resulting from the spatial derivative approximations. The difference between the semi-implicit and implicit algorithms is therefore the result of the time discretization error in the geostrophic balance. We see roughly one order of magnitude difference in the errors at the end of a five day simulation. The implicit method does not improve as the time step is decreased indicating that the dominant error for (IM) is the result of the semi-Lagrangian interpolations. As such it should be sensitive to horizontal resolution where the (SI) error should not improve with horizontal resolution.

Table 7 shows the error with increased horizontal resolution. Spectral T42 is used to approximate derivatives and the semi-Lagrangian interpolation uses twice as many points in each direction. The blank entries indicate a failure to converge to the desired tolerance for the implicit methods or a stability problem for the explicit methods. At T42 the explicit method can be stably integrated for 5 days using a time step of 600 seconds. The error in this case is $5.3e-4$ for the normalized ϕ integral and $6.3e-3$ for the normalized velocity error. This raises the question of whether the explicit method with a small time step is not to be prefered to the implicit methods.

It is rather striking that the semi-implicit algorithm does not converge for the large timestep. The failure manifests in the iterative solution where the residual is not reduced to the specified tolerance, the square root of machine epsilon. This failure occurs in the iterative solver when a poorly

	$\Delta t = 1200$			$\Delta t = 1800$		
Method	$nI(\phi)$	$nI(\mathbf{v})$	Iterations	$nI(\phi)$	$nI(\mathbf{v})$	Iterations
EX-SA*	-	-	-	-	-	-
EX-MID*	-	-	-	-	-	-
SI-SA*	1.9e-3	6.9e-2	10	-	-	-
SI-MID*	8.7e-3	6.5e-2	10	-	-	-
IM-SA	6.7e-3	3.2e-2	12	1.5e-3	2.0e-2	14
IM-MID	7.9e-4	6.3e-3	12	2.8e-3	2.4e-2	14

Figure 7: Case 2: Error Summary at 5 days, T42

	$\Delta t = 1200$			$\Delta t = 1800$		
Method	$nI(\phi)$	$nI(\mathbf{v})$	Iterations	$nI(\phi)$	$nI(\mathbf{v})$	Iterations
EX-SA*	-	-	-	-	-	-
EX-MID*	-	-	-	-	-	-
SI-SA*	3.4e-3	6.1e-2	11	1.4e-2	6.6e-2	20
SI-MID*	3.4e-3	6.1e-2	11	1.5e-2	6.6e-2	20
IM-SA	4.6e-4	1.0e-2	8	7.3e-4	1.5e-2	13
IM-MID	3.5e-4	4.0e-3	9	5.1e-4	3.7e-3	13

Figure 8: Case 3: Error Summary at 5 days, T42

conditioned matrix is used. A direct solver, or the spectral Helmholtz solution method, would not suffer a breakdown. But the direct solvers might return an inaccurate solution.

6.3 Steady State Zonal Flow with Compact Support

Test case 3, is similar to test case 2, but because the flow has compact support, it cannot be exactly representable by the sphercial harmonic expansion. Thus, errors in the spatial approximation of the derivatives are important. What we see in Table 8 that this error is predominant at T42. and the truncation errors due to the time stepping method are lost. The explicit method diverged for the time steps shown in Table 8. For $\Delta t = 600$ seconds it integrates stably and gives a normalized L2-error in geopotential of $2.7e-4$ and $4.7e-4$ in velocity.

For the time filtered equations there is apparently not much difference

Resolution	$\Delta t = 1800$	$\Delta t = 1200$	$\Delta t = 600$	$\Delta t = 300$
T10	6.9e-2	7.1e-2	5.9e-2	6.6e-2
T21	4.6e-4	3.1e-4	2.4e-4	2.5e-4
T42	4.6e-4	3.1e-4	1.3e-4	7.1e-5
T63	4.6e-4	3.0e-4	1.3e-4	7.1e-5

Figure 9: Case 3: Max. Velocity Error Summary at 1.67 hours, EX-MID

between the spatial average (SA) and mid-point (MID) splittings. For the implicit methods there seems to be a small advantage with the mid-point rule. The difference between the semi-implicit (SI) and implicit (IM) methods also seems to indicate that the geostrophic terms are best approximated together. Also note that the number of iterations required by the iterative method is larger for the semi-implicit algorithm than for the implicit algorithm.

Table 9 shows the max velocity error for different resolutions and differing timesteps. The method is the explicit midpoint. The consistency of the method is apparent even though for long time integrations stability will be a problem with the large timesteps. The spectral approximation to the derivatives is seen to improve with resolution to a point. This indicates that the spatial approximation error is less than the time truncation and spliting errors for the higher resolutions. With small timesteps, and hence small time truncation errors, the error is dominated by the spatial errors. If one is using a timestep of $\Delta t = 1800$ seconds, then resolution past T21 seems to be wasted. On the other hand, for a high spatial resolution of T63, the time and splitting errors are the limiting and must be considered carefully.

6.4 Rossby-Haurwitz Wave

For this case, no analytic solution is availabe. We will use this case to exhibit the conservation properties of the method.

7 Conclusions

The SLT algorithm is an important component of global atmospheric circulation models, and will be even more important in the next generation of models. Increased usage of the SLT technique promises both improved numerical accuracy and longer timesteps. However, effective utilization of the technique requires that accurate, efficient parallel implementations be developed. Since the SLT is only one component in the models, it is important that these implementations be evaluated in the context in which they will be used.

References

[1] J. R. Bates, F. H. M. Semazzi, R. W. Higgins, and S.R.M. Barros. Integration of the shallow water equations on the sphere using a vector semi-Lagrangian scheme with a multigrid solver. *Mon. Wea. Rev.*, 118:1615–1627, 1990.

[2] R.W. Freund. A transpose-free quasi-minimal residual algorithm for non-Hermitian linear systems. *SIAM J. on Sci. Comput.*, 14:470–482, 1993.

[3] R.W. Freund, M.H. Gutknecht, and N.M. Nachtigal. An implementation of the look-ahead Lanczos algorithm for non-Hermitian matrices. *SIAM J. on Sci. Comput.*, 14:137–158, 1993.

[4] R.W. Freund and N.M. Nachtigal. Qmr: a quasi-minimal residual method for non-hermitian linear systems. *Numer. Math.*, 60:315–339, 1991.

[5] R.W. Freund and N.M. Nachtigal. An implementation of the QMR method based on coupled two-term recurrences. *SIAM J. on Sci. Comput.*, 15:313–337, 1994.

[6] G. H. Golub and C. F. Van Loan. *Matrix Computations.* The John Hopkins University Press, Baltimore, Maryland, 1983.

[7] J.J. Hack R. Jakob and D.L. Williamson. Reference solutions to shallow water test set using the spectral transform method. Ncar tech note, National Center for Atmospheric Research, Boulder, CO, in preparation.

[8] H. Ritchie. Application of the semi-lagrangian method to a spectral model fo the shallow water equations. *Mon. Wea. Rev.*, pages 1587–1598, 1988.

[9] A. Staniforth and J. Côté. Semi-lagrangian integration schemes for atmospheric models – a review. *Mon. Wea. Rev.*, 119:2206–2223, 1991.

[10] M. Tanguay, E. Yakimiw, H. Ritchie, and A. Robert. Advantages of spatial averging in semi-implicit semi-lagrangian schemes. *Mon. Wea. Rev.*, pages 113–123, 1992.

[11] D. L. Williamson, J.B. Drake, J.J. Hack, Rudiger Jakob, and P.N. Swarztrauber. A standard test set for numerical approximations to the shallow water equations on the sphere. *J. Comp. Phys.*, pages 211–224, 1992.

[12] D. L. Williamson and J.G. Olson. Climate simulations with a semi-lagrangian version of the ncar community climate model. *Mon. Wea. Rev.*, pages 1594–1610, 1994.

[13] D. L. Williamson and P. J. Rasch. Two-dimensional semi-Lagrangian transport with shape-preserving interpolation. *Mon. Wea. Rev.*, 117:102–129, 1989.